A polynomial chaos method for arbitrary random inputs using B-splines

Christoph Eckert[a,*], Michael Beer[a,b,c], Pol D. Spanos[d]

[a] *Institute for Risk and Reliability, Leibniz University Hannover, Callinstr. 34, 30167 Hannover, Germany*
[b] *Institute for Risk and Uncertainty and School of Engineering, University of Liverpool, Peach Street, Liverpool L69 7ZF, UK*
[c] *International Joint Research Center for Engineering Reliability and Stochastic Mechanics, Tongji University, No.1239, Si Ping Rd, Shanghai 200092, China*
[d] *Lewis B. Ryon Professor in Mechanical and Civil Engineering, Rice University, P.O. Box 1892, Houston, TX 77251, USA*

Abstract

Isogeometric analysis which extends the finite element method through the usage of B-splines has become well established in engineering analysis and design procedures. In this paper, this concept is considered in context with the methodology of polynomial chaos as applied to computational stochastic mechanics. In this regard it is noted that many random processes used in several applications can be approximated by the chaos representation by truncating the associated series expansion. Ordinarily, the basis of these series are orthogonal Hermite polynomials which are replaced by B-spline basis functions. Further, the convergence of the B-spline chaos is presented and substantiated by numerical results. Furthermore, it is pointed out, that the B-spline expansion is a generalization of the Legendre multi-element generalized polynomial chaos expansion, which is proven by solving several stochastic differential equations.

Keywords: B-spline chaos, isogeometric basis, multi-element generalized polynomial chaos, approximation of arbitrary random variables, stochastic Galerkin

1. Introduction

The usage of polynomial chaos (PC) representations to approximate random processes is widespread in the area of stochastic mechanics (e.g. [1, 2, 3, 4]), and has a mathematically solid framework. For any arbitrary random process with finite second-order moments the original Wiener polynomial chaos expansion [5] converges in accord with the Cameron-Martin theorem [6]. Further, the convergence rate is optimal for Gaussian inputs; in fact the rate is exponential [7]. This can be understood from the fact that the weighting function of Hermite polynomials is the same as the probability density function of the Gaussian random variables. For other types of random input the convergence rate may substantially slower. In this case, other types of orthogonal polynomials, instead of Hermite polynomials, could be used to construct the chaos expansion. Xiu and Karniadakis [7] proposed the generalized polynomial chaos (gPC) and proved optimal convergence for the polynomials of the Askey-scheme, e.g. Legendre polynomials correspond to the uniform distribution. Further, Wan and Karniadakis [8] extended the gPC by decomposing the stochastic space in elements and build a gPC within each element, which is known as the multi-element generalized polynomial chaos (ME-gPC). This extension captures the problems of long-term integration and stochastic discontinuities, and was especially applied to flow problems [9, 10] and others [11, 12, 13, 14]. More recently, improvements of the method were proposed [15, 16], but handling long-term integration and stochastic discontinuities remains a challenging problem.

The original Wiener and the generalized PC have also been successfully applied to arbitrary non-optimal inputs [17]. [3] However, in practical applications, one often does not know the analytical form of the distribution of the input, or, if known, it may not be one of the classical distributions, e.g. uniform, Gaussian, exponential, etc. In this case, the optimal convergence may deteriorates [4, 18], especially for higher orders.

In 2005, Hughes et al. [19] bridged the gap between computer aided design and engineering by introducing the methodology of isogeometric analysis (IGA), which successfully has enhanced many deterministic engineering applications [20, 21, 22, 23, 24]. In this regard, it is remarkable that the notion of IGA was not widely adopted within stochastic frameworks [25, 26, 27]. In the best of the authors' knowledge, there are two relevant approaches: Hien and Noh [26] combined the IGA with stochastic perturbation and Li et al. [27] numerically solved the Karhunen-Love expansion using isogeometric basis functions. One procedure within the IGA framework is to use non-uniform rational B-Splines (NURBS), which are prevalent in engineering design processes, as a basis for solution fields. It turned out that B-splines are also beneficial in terms of the analysis.

*Corresponding author
Email addresses: eckert@irz.uni-hannover.de (Christoph Eckert), beer@irz.uni-hannover.de (Michael Beer), spanos@rice.edu (Pol D. Spanos)

In this paper, the B-spline basis functions are employed in the truncated PC expansion and weak convergence for arbitrary input variables are shown. Further, strong convergence is achieved for uniform distributed random inputs. These results are supported by numerical examples where approximations of beta, normal, and exponential distribution are extensively studied and compared with Hermite and Legendre chaos. Afterwards, a first order ordinary differential equation (ODE) and a cantilever Euler-Bernoulli beam with random flexural rigidity is solved by B-spline expansions using a stochastic Galerkin scheme and faced with Legendre chaos.

2. Wiener-Askey chaos

Let $(\Omega, \mathcal{F}, \mathcal{P})$ be a probability space, where Ω is a sample space, $\mathcal{F}$ is an appropriate σ-field on Ω, $\mathcal{P}$ is a probability measure and $(\mathbb{R}, \mathcal{B})$ a measurable space, where $\mathcal{B}$ is the Borel σ-field. A (real-valued) random variable X on $(\Omega, \mathcal{F}, \mathcal{P})$ is an mapping $X : \Omega \to \mathbb{R}$ which is $(\mathcal{F}, \mathcal{B})$-measurable. Denote by $L_2(\Omega, \mathcal{F}, \mathcal{P})$ the Hilbert space of all random variables with finite second moment, i.e. $\mathbf{E}[X^2] < \infty$ with $\mathbf{E}[\cdot]$ is the operator of mathematical expectation. Consider the random variable X as a function of an arbitrary random variable Z, i.e.

$$X = g(Z), \tag{1}$$

where g is a deterministic, measurable mapping. In general, equation (1) describes the random output X of a stochastic system in the presents of random inputs, parameterized by a set of independent variables Z.

Wiener [5] proposed the Hermite PC which allows to represent equation (1) in terms of the series

$$X = \sum_{p=0}^{\infty} a_p H_p(Z), \tag{2}$$

where Z is Gaussian, $H_p(Z)$ are Hermite polynomials in Z of order p and a_p are deterministic coefficients to be determined. Truncating the series in equation (2) after the $P+1$ term leads to the PC approximation of order P:

$$\tilde{X}_P = \sum_{p=0}^{P} a_p H_p(Z) \tag{3}$$

which converges in $L_2(\Omega, \mathcal{F}, \mathcal{P})$ [1], i.e.

$$\tilde{X}_P \xrightarrow{L_2} X \quad \text{for} \quad P \to \infty. \tag{4}$$

Due to the orthogonality of the Hermite functions, the coefficients in (3) can simply determined by the orthogonal L_2 projection

$$\mathbf{E}[g(Z)H_p(Z)] = a_p \, \mathbf{E}[H_p(Z)^2] \tag{5}$$

for every p, which make these polynomials very efficient for computational issues. The orthogonality depends on the measure $\mathcal{P}$ of $L_2(\Omega, \mathcal{F}, \mathcal{P})$ and in the above case a Gaussian measure is at the basis of L_2. The convergence property guarantees the effectiveness of solving stochastic differential equations with Gaussian inputs [1, 2].

It has been demonstrated by many authors that the Hermite chaos is effective in solving stochastic differential equations with Gaussian inputs as well as certain types of non-Gaussian inputs [28, 1, 29, 4]. Nevertheless, the optimal exponential convergence rate is not achieved for general non-Gaussian random inputs or the convergence severely deteriorates [7, 18]. Xiu and Karniadakis [7] proposed the Wiener-Askey or generalized polynomial chaos in 2002:

$$X = \sum_{p=0}^{\infty} a_p \Psi_p(Z). \tag{6}$$

It identifies a correspondence between the distribution of the random input Z and the type of orthogonal polynomials Ψ form the Askey scheme of hypergeometric orthogonal polynomials, which leads to optimal convergence rates, i.e. exponentially. Some elected correspondences are shown in table 1 - e.g. [28].

Distribution of Z	Polynomial Basis Ψ	Support
Gaussian	Hermite	$(-\infty, \infty)$
Gamma	Laguerre	$[0, \infty)$
Beta	Jacobi	$[a, b] \subset \mathbb{R}$
Uniform	Legendre	$[a, b] \subset \mathbb{R}$

Table 1: Correspondence between distribution and polynomial basis.

3. B-spline chaos

In this section, the PC approximation is adapted in order to make the method accessible for B-spline basis functions instead of orthogonal polynomials. B-spline basis functions, which are piecewise Bernstein polynomials, are characterized by an open non-uniform knot vector

$$\begin{aligned} \Xi &= [\underbrace{0, \ldots, 0}_{p+1}, u_{p+2}, \ldots, u_N, \underbrace{1, \ldots, 1}_{p+1}] \\ &= [u_1, \ldots, u_{N+p+1}] \end{aligned} \tag{7}$$

where p is the polynomial order and N is the number of basis functions - e.g. [19]. The u_i's are called knots and define element boundaries if they differ. The B-spline basis functions can then be explained by the Cox-de Boor recursion formula:

$$B_{i,p}(u) := \begin{cases} 1 & \text{if} \quad u_i \le u < u_{i+1} \\ 0 & \text{otherwise} \end{cases} \tag{8}$$

for $p = 0$, and

$$\begin{aligned} B_{i,p}(u) :=& \frac{u - u_i}{u_{i+p} - u_i} B_{i,p-1}(u) \\ &+ \frac{u_{i+p+1} - u}{u_{i+p+1} - u_{i+1}} B_{i+1,p-1}(u) \end{aligned} \tag{9}$$

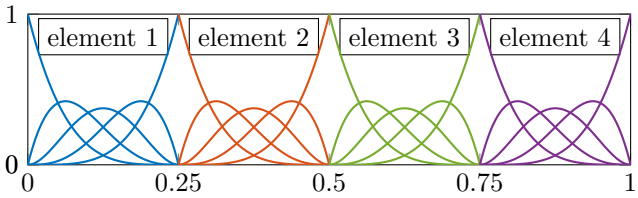

Figure 1: B-spline basis of order $p = 4$ with knot vector $\Xi = [0, 0, 0, 0, 1/4, 1/4, 1/4, 1/2, 1/2, 1/2, 3/4, 3/4, 3/4, 1, 1, 1, 1]$ leading to four $\mathcal{C}^0$-elements with $N = 17$ basis functions.

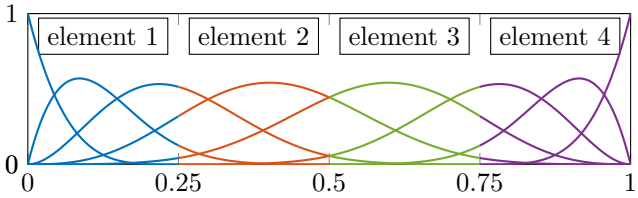

Figure 2: B-spline basis of order $p = 4$ with knot vector $\Xi = [0, 0, 0, 0, 1/4, 1/2, 3/4, , 1, 1, 1, 1]$ leading to four $\mathcal{C}^3$-elements with $N = 8$ basis functions.

for $p \geq 1$. Repeating inner knots in the interior of the knot vector entail in a lower continuity over element boundaries. Single knots reveal a $\mathcal{C}^{p-1}$-continuity. This can be seen in Fig. 1 and Fig. 2, respectively. A prescribed continuity affects profoundly the number of basis functions, too. This indeed is the main reason for the effectiveness of the subsequent method.

Denote by $B_{i,p}(u)$ the i-th B-spline basis function of order p defined on $[0, 1]$ with $i = 1, \ldots, N$. According to the original Wiener polynomial chaos, the B-spline chaos of order p and knot vector Ξ is defined by

$$\tilde{X}_N = \sum_{i=1}^{N} x_i B_{i,p}(u(Z)). \tag{10}$$

B-splines can not be used for the approximation of random variables in the same manner then orthogonal polynomials, like Hermite polynomials, because of the lack of orthogonality. Nevertheless, it suffices that the functions in use form a basis of the underlying Hilbert space $L_2(\Omega, \mathcal{F}, \mathcal{P})$ [1, 28]. Thus, the coefficients in (10) can be determined by solving a linear algebraic system resulting from the L_2 projection:

$$\mathbf{A}\mathbf{x} = \mathbf{b} \tag{11}$$

with

$$\mathbf{A}_{i,j} := \mathbf{E}\left[B_{i,p}(u(Z))B_{j,p}(u(Z))\right] \tag{12}$$
$$\mathbf{b}_j := \mathbf{E}\left[g(Z)B_{j,p}(u(Z))\right] \tag{13}$$

$i, j = 1, \ldots, N$. Next, the integrals in equation (11) must be calculated. Specifically, this necessitates the introduction of a new space for the parameter u of the B-spline basis functions $B_{i,p}(u(Z))$, which explicitly depend on the random variable Z. The question next arises as to how an arbitrary random variable Z can be uniquely mapped on the parameter space $[0, 1]$ in a proper way. A convenient choice is the inverse cumulative distribution function (CDF) of a random variable Z, given by

$$F_Z^{-1}(u) := \inf\{z \ : \ F_Z(z) \geq u\} \in [0, 1], \tag{14}$$

where F_Z is the CDF of Z. Clearly, the inverse always exists and is unique. This allows one to connect the parameter u and the random variable Z such that u become a uniformly distributed random variable $U = F_Z(Z)$ on the interval $[0, 1]$, i.e.

$$\begin{aligned} F_U(u) &= P(U \leq u) = P(F_Z(Z) \leq u) \\ &= P(Z \leq F_Z^{-1}(u)) = F_Z(F_Z^{-1}(u)) = u \\ \implies & U \sim \mathcal{U}([0, 1]). \end{aligned} \tag{15}$$

If the distribution of Z is explicitly known, equation (11) can be expressed in terms of U by

$$u = F_Z(z) \quad \implies \quad \frac{du}{dz} = \frac{dF_Z(z)}{dz} = f_Z(z), \tag{16}$$

where f_Z is the probability density function of Z. Hence, a proper mapping between Ω and $[0, 1]$ by F_Z is established. So, the expressions in (12) and (13) can be expressed as

$$\begin{aligned} &\mathbf{E}_Z\left[B_{i,p}(F_Z(Z))B_{j,p}(F_Z(Z))\right] \\ &\quad = \int_\Omega B_{i,p}(F_Z(z))B_{j,p}(F_Z(z))f_Z(z)\ dz \\ &\quad = \int_{[0,1]} B_{i,p}(u)B_{j,p}(u)\ du \\ &\quad = \mathbf{E}_U\left[B_{i,p}(U)B_{j,p}(U)\right], \end{aligned} \tag{17}$$

and

$$\begin{aligned} &\mathbf{E}_Z\left[g(Z)B_{j,p}(F_Z(Z))\right] \\ &\quad = \int_\Omega g(z)B_{j,p}(F_Z(z))f_Z(z)\ dz \\ &\quad = \int_{[0,1]} g(F_Z^{-1}(u))B_{j,p}(u)\ du \\ &\quad = \mathbf{E}_U\left[g(F_Z^{-1}(U))B_{j,p}(U)\right]. \end{aligned} \tag{18}$$

Thus, the matrix $\mathbf{A}$ depends only on the configuration of the B-spline basis functions, and can be stored before the analysis. Further, $\mathbf{A}$ is a band matrix, if the knot vector Ξ has inner knots, i.e.

$$\mathbf{A}_{i,j} = 0 \quad \text{for} \quad |i - j| > p + 1. \tag{19}$$

Examining the integrals in (17) and (18) it turns out that only the inverse cumulative distribution function of the describing random variable Z and the mapping g must be known. Thus, this procedure is not strongly limited and simultaneously paves the way for using this method with discrete random variables. Besides, under the assumption that Z is a uniformly distributed random variable F_Z is the identity, and optimal convergence is expected in correspondence with the uniform distribution, which is shown in the ensuing section.

3.1. Convergence

The proposed method is closely related to the gPC [7] where the same mapping property between a uniform and arbitrary distribution is utilized. It can be shown, see e.g. [28], that the gPC approximation converges weakly, if the random variable to be approximated is square integrable and the moments in the chaos expansion exists. This can be adopted here and $\tilde{X}_N$ converges in probability and in distribution, i.e.

$$\tilde{X}_N \xrightarrow{\mathcal{P}} X \text{ and } \tilde{X}_N \xrightarrow{\mathcal{D}} X \quad \text{for} \quad N \to \infty. \tag{20}$$

To be precise, this can be stated as follows:

Definition 1 (Weak chaos approximation)**.** *Let X be a random variable with CDF $F_X(x) = \mathcal{P}(X \leq x)$ and let Z be an arbitrary random variable in a set of basis functions $\Psi_i(Z)$, $i = 1, \ldots, N$. If*

$$\tilde{X}_N = \sum_{i=1}^{N} a_i \Psi_i(Z) \quad \textit{with } a_i \in \mathbb{R} \tag{21}$$

converges to X in a weak sense, i.e.

$$\tilde{X}_N \xrightarrow{\mathcal{P}} X \textit{ or } \tilde{X}_N \xrightarrow{\mathcal{D}} X \quad \textit{for} \quad N \to \infty, \tag{22}$$

then $\tilde{X}_N$ is a weak chaos approximation of X.

Theorem 1. *Let X be a random variable with CDF $F_X(x) = \mathcal{P}(X \leq x)$ and finite second moment. Let U be a uniformly distributed random variable in $[0, 1]$ such that the moments $\mathbf{E}_U(B_{i,p}(U)B_{j,p}(U))$ exists for all B-spline basis functions of order $p \in \mathbb{N}$ with $i, j \in \{1, \ldots, N\}$. Let*

$$\tilde{X}_N = \sum_{i=1}^{N} x_i B_{i,p}(U) \tag{23}$$

the weak B-spline chaos approximation of X, where $\mathbf{x} = (x_1, \ldots, x_N)$ results from the L_2 projection $\mathbf{Ax} = \mathbf{b}$ with

$$\mathbf{A}_{i,j} := \mathbf{E}_U \left(B_{i,p}(U) B_{j,p}(U) \right) \quad \textit{and} \tag{24}$$

$$\mathbf{b}_j := \mathbf{E}_U (F_X^{-1}(U) B_{j,p}(U)). \tag{25}$$

Then $\tilde{X}_N$ converges to X in probability, i.e.

$$\tilde{X}_N \xrightarrow{\mathcal{P}} X \quad \textit{for} \quad N \to \infty. \tag{26}$$

Proof. Let

$$\bar{X} := F_X^{-1}(U) = F_X^{-1}(F_U(U)), \tag{27}$$

which implies that $\bar{X}$ has the same probability distribution as X, i.e. $F_{\bar{X}} = F_X$. Thus, it holds $\bar{X} \overset{\mathcal{P}}{=} X$ and $\mathbf{E}(\bar{X}^2) < \infty$, which leads to

$$\begin{aligned} \infty > \mathbf{E}\left[\bar{X}^2\right] &= \int_{\Omega_X} x^2 \, dF_X(x) \\ &= \int_{[0,1]} \left(F_X^{-1}(u)\right)^2 \, du \\ &= \int_{[0,1]} \left(F_X^{-1}(F_U(u))\right)^2 \, dF_U(u). \end{aligned} \tag{28}$$

$$\begin{aligned} \implies \quad & \bar{X} \in L_2([0,1], \sigma([0,1]), dF_U) \\ & := \left\{ f : [0,1] \to \mathbb{R} \mid \mathbf{E}_U\left[f^2\right] < \infty \right\}. \end{aligned} \tag{29}$$

Since (23) is the L_2 projection of $\bar{X}$ by $\tilde{X}_N$, $\tilde{X}_N$ converges in mean square to $\bar{X}$, which implies

$$\tilde{X}_N \xrightarrow{\mathcal{P}} \bar{X} \qquad \text{for} \quad N \to \infty. \tag{30}$$

This completes the proof, because $\bar{X} \overset{\mathcal{P}}{=} X$. □

Note, convergence in probability implies convergence in distribution. So, it also holds $\tilde{X}_N \xrightarrow{\mathcal{D}} X$ for $N \to \infty$. Further, if $g(Z)$ in equation (1) is explicitly known in terms of Z, L_2 convergence can be achieved [28]. However, in most practical numerical analyses only the probability density function of $g(Z)$ or even less information is available. But in this case, strong convergence can not established because of the lack of information concerning g and Z. Nevertheless, the above theorem ensures weak convergence.

4. Numerical examples

In this section the versatility of the aforementioned approach is demonstrated, and the convergence results are further substantiated by numerical examples. First, several random variables are approximated by different expansions and are juxtaposed with each other. Finally, a first order stochastic differential equation and a cantilever beam are solved using a stochastic Galerkin scheme and compared to the Legendre multi-element chaos. Besides, *h-p* convergence is shown and it turns out, that the B-spline chaos is a generalization of the Legendre multi-element polynomial chaos, which can extensively improved by increasing the continuity over stochastic element boundaries.

4.1. Approximation of random variables

In the following uniform, beta, normal, and exponential distributed random variables are approximated by Hermite, Legendre and B-spline chaos. The resulting density functions are estimated by a normal kernel smoothing function available in all common statistical toolboxes[1]. The advantage of the proposed technique lies in the flexibility of adapting the order, number of elements and continuity over element boundaries, which can be quite powerful if the underlying distribution is unknown.

4.1.1. Uniform distribution

Fig. 3 shows approximations of a uniform density function by Hermite, Legendre, and B-spline chaos for different orders p. Legendre and B-spline expansions remain stable and unchanged from the first order on. Neither order elevation nor knot insertion changes the accuracy. The

[1]For the presented examples the ksdensity MATLAB-function with bandwidth 0.06 and 1.000.000 samples were used.

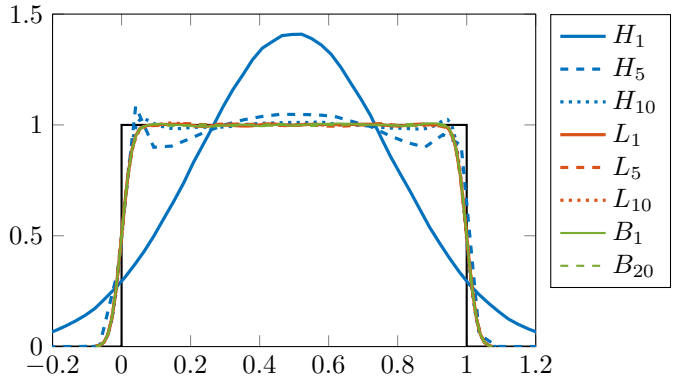

Figure 3: Approximations of a uniform distribution by Hermite polynomials (H_p), Legendre polynomials (L_p), and B-splines (B_p).

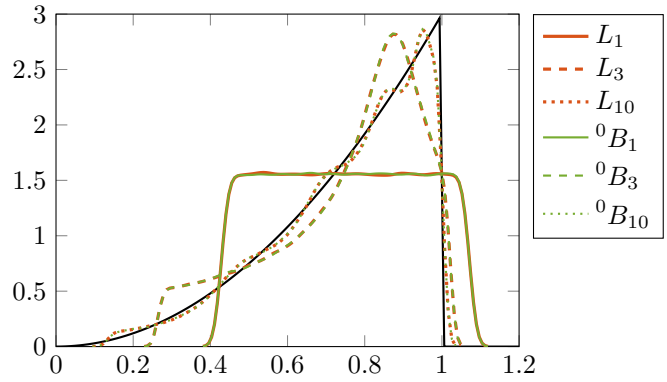

Figure 5: Approximations of a beta distribution with $\alpha = 3$ and $\beta = 1$ by Legendre polynomials (L_p) and $\mathcal{C}^0$ B-splines (${}^0B_p$).

changing values of the expansion coefficients are the main difference. While only the first two basis functions influence the representation for the Legendre chaos, because all coefficients are zero for $i > 2$, the coefficients are changing for every configuration for the B-splines - see Fig. 4. However, in this case only a straight line has to be approximated. Therefore, linear B-splines are sufficient. This leads to the conclusion that a correspondence between the uniform distribution and B-splines can be identified. However, for the Hermite chaos more terms are necessary to reach the same accuracy, and oscillations are observed at the corners. This is also known as the stochastic Gibbs phenomenon [28].

4.1.2. Beta distribution

Let X be a beta distributed random variable on $[0, 1]$ with density function

$$f_X(x) = \frac{1}{\mathrm{B}(\alpha, \beta)} x^{\alpha-1}(1-x)^{\beta-1} \quad \text{with } \alpha, \beta > 0\,, \tag{31}$$

where $\mathrm{B}(\alpha, \beta)$ is the beta function. Results of for a beta distributed random variable X with $\alpha = 3$ and $\beta = 1$ are shown in Fig. 5. Legendre and Bernstein ($\mathcal{C}^0$ B-spline)

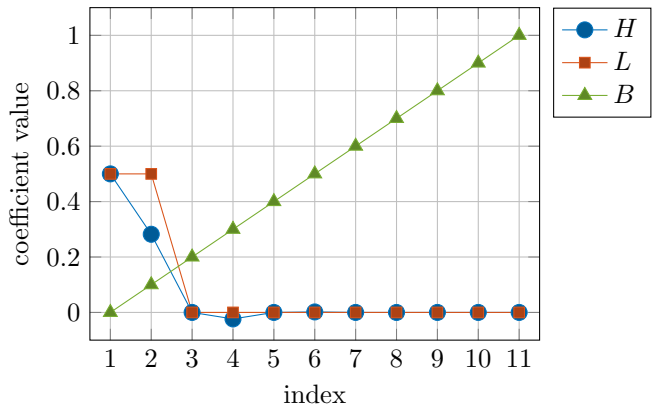

Figure 4: Coefficient values of Hermite, Legendre, and B-spline chaos for approximating a uniformly distributed random variable.

approximations are compared, for which an explicit one-to-one transformation exists [30]. A further indication for the connection of Legendre and Bernstein polynomials is the indistinguishableness of the illustrated results. However, the approximations could be substantially improved by adding inner knots. Then, the Bernstein polynomials become B-splines basis functions.

4.1.3. Normal distribution

Let $X \sim \mathcal{N}(\mu, \sigma^2)$ be a normal distributed random variable with density function

$$f_X(x) = \frac{1}{\sqrt{2\pi\ \sigma^2}}\ \exp\left(-\frac{(x-\mu)^2}{\sigma^2}\right) \tag{32}$$

with expectation $\mu \in \mathbb{R}$ and variance $\sigma^2 > 0$. Hermite polynomials correspond to the Gaussian measure. Thus, the Hermite chaos is exact from the first order on - see Fig. 6. Further, a Gaussian kernel is used here. Thus, the approximation fits perfectly. In contrast, a Gaussian input is not optimal for the B-spline or Legendre chaos, which can clearly be recognized. Nevertheless, inserting nine inner knots, which leads to ten stochastic elements, improves the performance distinctly, although moderate oscillations remain at the tails. The fluctuations can be attributed to the different supports. The L_2 projection must determine a proper mapping from $[0, 1]$ to $(-\infty, \infty)$.

4.1.4. Exponential distribution

Assume that X is a exponential distributed random variable on $[0, \infty]$ with density function

$$f_X(x) = \lambda \exp(-\lambda) \quad \text{with } \lambda > 0 \tag{33}$$

and consider the specific case of $\lambda = 1$. The Hermite chaos behaves quite well for higher orders and is smooth, although the peak decreases for $P = 10$ - see Fig. 7. As seen before, nine inner knots are utilized in order to diminish the oscillations for the B-splines, but the deviation remains fairly large on the right end. Now, another useful property of B-spline basis functions can be exploited

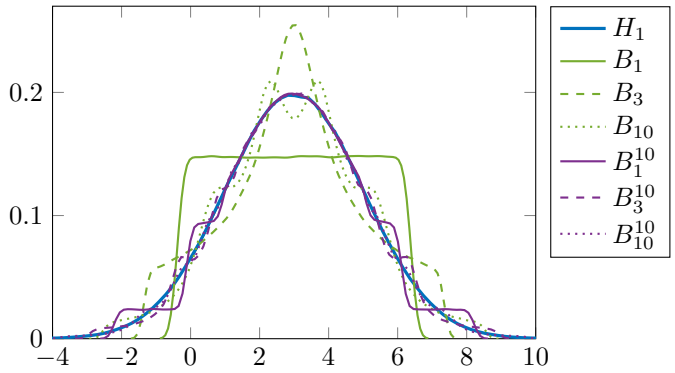

Figure 6: Approximations of a normal distribution with $\mu = 3$ and $\sigma = 2$ by Hermite polynomials (H_p) and B-splines with ten stochastic elements (B_p^{10}).

to solve this issue. Inserting the same knot again reduces the continuity over element boundaries by one. This can be repeated until the B-splines become decomposed, i.e. $\mathcal{C}^0$-continuity over element boundaries. In Fig. 7, ${}^0B_{10}^{10}$ specifies the case for ten $\mathcal{C}^0$-elements of order ten, which leads to a much smoother approximation and can compete against the Hermite chaos. Solely, the tail is slightly fluctuating which may be caused by the support mismatch. Further, the employed normal kernel smoothing function is non-optimal for the B-splines representation.

4.2. First order stochastic ordinary differential equation

In the following consider the stochastic ODE from Wan and Karniadakis [8]

$$\frac{\mathrm{d}\, y(t)}{\mathrm{d}\, t} = -a\, y(t) \quad \text{with} \quad y(0) = 1, \tag{34}$$

where $t \in \mathbb{R}_+$ and the decay rate $a : \Omega \to \mathbb{R}$ is a random variable with mean μ_a and density function f_a. The exact solution of (34) is

$$y(t) = \exp(-a(\omega)\, t). \tag{35}$$

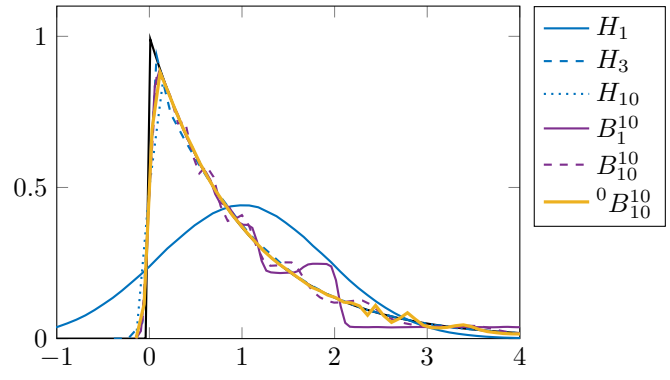

Figure 7: Approximations of a exponential distribution with $\lambda = 1$ by Hermite polynomials (H_p), B-splines with ten elements (B_p^{10}), and $\mathcal{C}^0$ B-splines with ten elements (${}^0B_p^{10}$)

Then, the stochastic mean solution can be determined by

$$\mathbf{E}\left[y(t)\right] = \int_S \exp(-at) f_a(a)\; da \tag{36}$$

with support S of a.
Applying the B-spline chaos to the random variables a and y yields

$$\tilde{a}^N = \sum_{i=1}^{N} a_i B_{i,p}(U) \tag{37}$$

and

$$\tilde{y}^N(t) = \sum_{i=1}^{N} y_i(t) B_{i,p}(U), \tag{38}$$

where $U \sim \mathcal{U}([0,1])$ corresponds to the B-spline basis. Substituting equation (37) in (34) leads to

$$\sum_{i=1}^{N} \frac{\mathrm{d}\, y_i(t)}{\mathrm{d}\, t} B_{i,p}(U) = -\sum_{i=1}^{N}\sum_{j=1}^{N} a_i y_j(t) B_{i,p}(U) B_{j,p}(U). \tag{39}$$

Applying the Galerkin projection to equation (39) yields

$$\sum_{i=1}^{N} \frac{\mathrm{d}\, y_i(t)}{\mathrm{d}\, t} \mathbf{E}\left[B_{i,p}(U)\, B_{k,p}(U)\right] = -\sum_{i=1}^{N}\sum_{j=1}^{N} a_i y_j(t)\, \mathbf{E}\left[B_{i,p}(U)\, B_{j,p}(U)\, B_{k,p}(U)\right] \tag{40}$$

$k = 1, \ldots, N$. The system of equations (40) can be solved by any ODE solver. Here, the standard fourth order Runge-Kutta scheme is used. For the mean and variance the errors are defined by

$$\varepsilon_{\text{mean}}(t) = \left| \frac{\mathbf{E}\left[\tilde{y}^N(t)\right] - \mathbf{E}\left[y(t)\right]}{\mathbf{E}\left[y(t)\right]} \right| \tag{41}$$

and

$$\varepsilon_{\text{var}}(t) = \left| \frac{\mathbf{Var}\left[\tilde{y}^N(t)\right] - \mathbf{Var}\left[y(t)\right]}{\mathbf{Var}\left[y(t)\right]} \right|, \tag{42}$$

where $\mathbf{Var}\left[y(t)\right] = \mathbf{E}\left[y(t) - \mathbf{E}\left[y(t)\right]^2\right]$.
In the sequel, the random decay rate is expected to be uniformly distributed, i.e. $a(\omega) \sim \mathcal{U}([-1,1])$. Thus, the exact stochastic mean solution is

$$\mathbf{E}\left[y(t)\right] = \frac{\sinh(t)}{t}. \tag{43}$$

Numerical results of equation (40) are shown in Fig. 8. Hermite, Legendre and B-spline representations are opposed against each other. Specifically, the relative mean

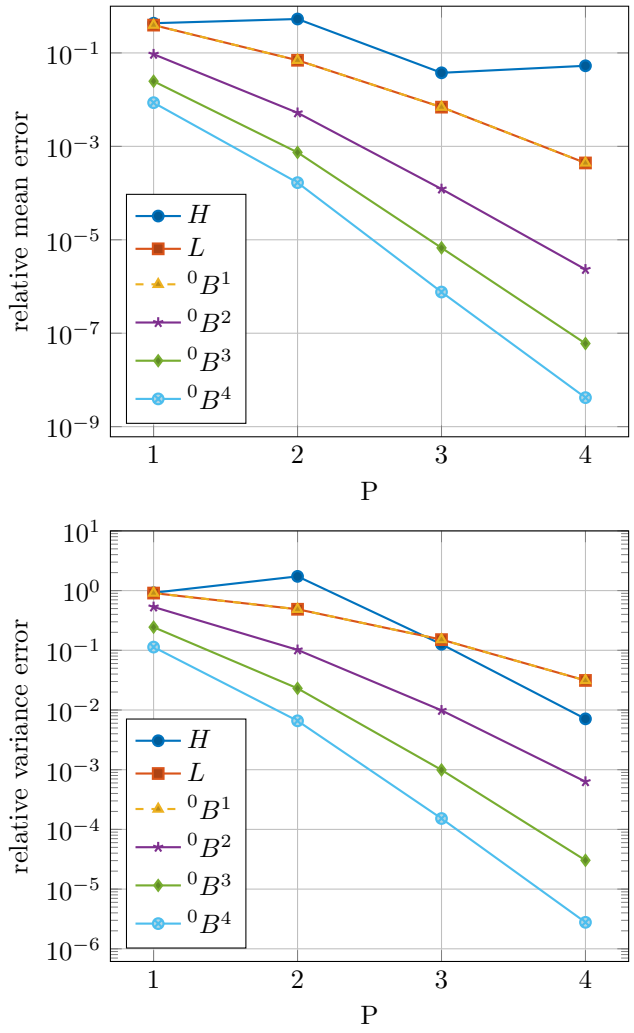

Figure 8: Relative mean and variance error of Hermite, Legendre, and B-spline chaos for $t = 5$.

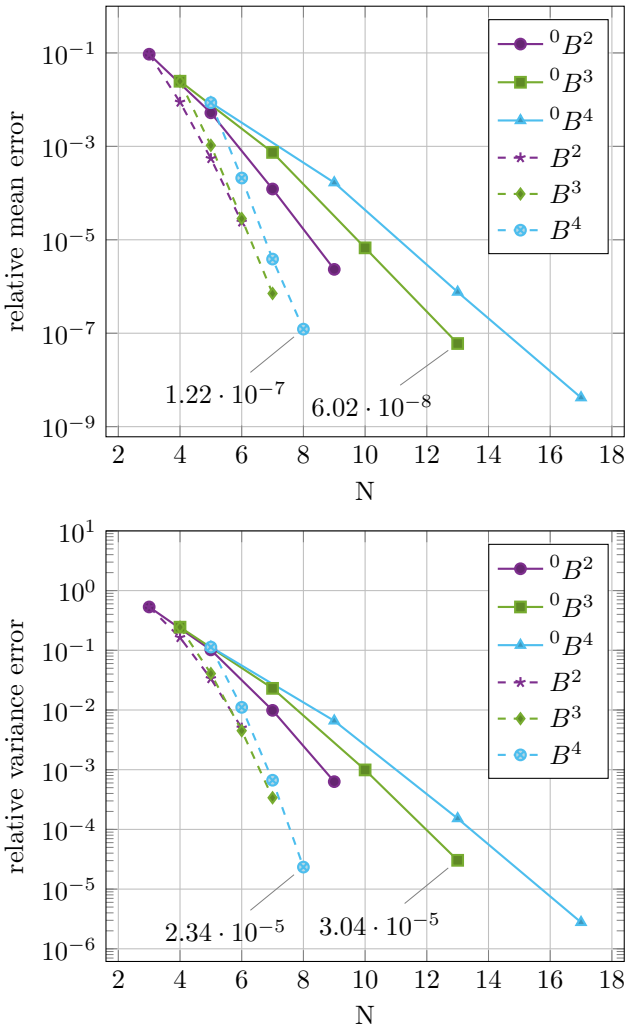

Figure 9: Relative mean and variance error of $\mathcal{C}^0$ and $\mathcal{C}^{p-1}$ B-spline chaos for $t = 5$.

and variance error of the multi-element generalized polynomial chaos from [8] are reproduced by using Bernstein polynomials, which are equivalent to $\mathcal{C}^0$ B-spline basis functions - see Fig. 1 for instance. Exponential p-type convergence for different stochastic meshes, i.e. number of elements in the spectral expansion, are achieved. The Legendre chaos is optimal for the uniform input. Therefore, it generally outperforms the Hermite chaos here, which error is fluctuating and decreases slowly. Furthermore, the Legendre multi-element approach coincides with the $\mathcal{C}^0$ B-spline chaos. Increasing the number of elements validates the results of Wan and Karniadakis [8, Fig. 2]. This means, through the natural structure of B-splines, that the performance of Legendre multi-element chaos is inherited by simply using $\mathcal{C}^0$ B-splines basis functions in the polynomial chaos expansion. Note in addition, it is much easier to implement the B-spline basis in an ordinary PC framework then it is the case with me-gPC.

Further, the capability of $\mathcal{C}^0$ with $\mathcal{C}^{p-1}$ B-spline chaos are compared. The convergence for the error of mean and variance of the solution with respect to the number of basis functions is illustrated in Fig. 9. The solid lines represent the same results as in Fig. 8, whereas the dashed lines show the errors of the $\mathcal{C}^3$ B-spline chaos. Exponential h-type convergence for both B-spline variants are on hand. Moreover, it can clearly be seen that for $\mathcal{C}^3$-continuity much less basis functions are needed to reach nearly the same accuracy. This crucial point is emphasized distinctly by the marked data sets. The marked data point of B^4 belongs to the basis functions shown in Fig. 2 with $N = 8$ and is competitive against the marked data point of ${}^0B^3$ with $N = 13$ for both error types. The number of basis functions N is directly related to the degrees of freedom of the numerical model. Thus, using smooth B-splines over element boundaries instead of Legendre polynomials in each element leads to a drastic reduction of the degrees of freedom and gain of efficiency. As mentioned above, this improvement is predicated on the smoothness over element boundaries. Note that, the exhibit advantages becomes even more pronounced if more elements or higher degrees

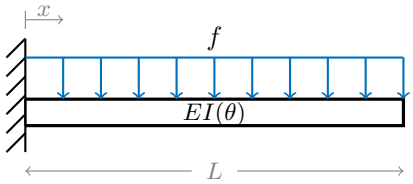

Figure 10: Cantilever Euler-Bernoulli beam with deterministic uniformly distributed load f and random beam rigidity $EI(\theta)$.

are treated.

4.3. Euler-Bernoulli beam with random stiffness

Next, consider the Euler-Bernoulli beam of length $L = 1$, clamped at $x = 0$, and subjected to a deterministic uniformly distributed load f shown in Fig. 10. The governing equation is given by

$$EI\ \frac{d^4}{dx^4}u(x) = f \quad \text{with} \quad u(0) = u'(0) = 0, \tag{44}$$

where the beam rigidity $W \equiv EI$ is assumed to be a random variable $W : \Omega \to \mathbb{R}$ with density function f_W, and is specified by the modulus of elasticity E and the area moment of inertia I. The exact solution of (44) reads

$$u(x,\theta) = f\ \frac{x^2(6L^2 - 4Lx + x^2)}{24\ EI(\theta)}. \tag{45}$$

In order to make equation (44) numerically feasible the spatial and stochastic space of the solution and the random input must be discretized. Using isogeometric subspace leads to

$$\begin{aligned}\tilde{u}(x,\theta) &= \sum_{l=1}^{n_d} u_l(\theta) N^d_{l,p_d}(u(x)) \\ &= \sum_{l=1}^{n_d}\sum_{i=1}^{n_s} u_{il} N^s_{i,p_s}(U(\theta)) N^d_{l,p_d}(u(x)),\end{aligned} \tag{46}$$

and

$$\widetilde{W}(\theta) = \sum_{k=1}^{n_w} w_k N^w_{k,p_w}(U(\theta)), \tag{47}$$

where $u(x)$ is a linear mapping from the spatial space $[0, L]$ and the parameter space $[0, 1]$, and $U : \Omega \to [0, 1]$ a uniformly distributed random variable, i.e. $U \sim \mathcal{U}([0, 1])$. Note, for the deterministic part classical Hermite basis functions can be used in the same way.
Applying the deterministic Galerkin procedure to equation (44) yields

$$\begin{aligned}&\sum_{l=1}^{n_d} u_l(\theta) \int_L \frac{d^2}{dx^2}N^d_{l,p_d}(x)\ W(\theta)\ \frac{d^2}{dx^2}N^d_{m,p_d}(x)\ dx \\ &\quad = \int_L f\ N^d_{m,p_d}(x)\ dx \quad m = 1,\dots,n_d \\ &\Leftrightarrow: \quad K^d(\theta)u^d(\theta) = f^d.\end{aligned} \tag{48}$$

Next, using equations (46) and (47), and applying the stochastic Galerkin procedure gives

$$\begin{aligned}&\sum_{l=1}^{n_d}\sum_{i=1}^{n_s}\sum_{k=1}^{n_w} u_{il} w_k\ \mathbf{E}_U\left[N^s_{i,p_s}(U) N^s_{j,p_s}(U) N^w_{k,p_w}(U)\right] \\ &\qquad \int_L \frac{d^2}{dx^2}N^d_{l,p_d}(x)\ \frac{d^2}{dx^2}N^d_{m,p_d}(x)\ dx \\ &\quad = \mathbf{E}_U\left[N^s_{j,p_s}(U)\right]\int_L f N^d_{m,p_d}(x)\ dx\end{aligned} \tag{49}$$

for $j = 1,\dots,n_s$ and $m = 1,\dots,n_d$ which can be reformulated in a matrix scheme of dimension $n_d n_s \times n_d n_s$:

$$Ku = f \tag{50}$$

with

$$\begin{aligned}K_{ijlm} &:= \underbrace{\sum_{k=1}^{n_w} w_k\ \mathbf{E}_U\left[N^s_{i,p_s}(U) N^s_{j,p_s}(U) N^w_{k,p_w}(U)\right]}_{=:K^s_{ijk}} \\ &\qquad \underbrace{\int_L \frac{d^2}{dx^2}N^d_{l,p_d}(x)\ \frac{d^2}{dx^2}N^d_{m,p_d}(x)\ dx}_{=:K^s_{lm}} \\ &= K^s_{ijk}K^s_{lm} \qquad \begin{matrix} i,j = 1,\dots,n_s \\ l,m = 1,\dots,n_d \end{matrix}\end{aligned} \tag{51}$$

and

$$\begin{aligned}f_{jm} &:= \underbrace{\mathbf{E}_U\left[N^s_{j,p_s}(U)\right]}_{f^s_j}\underbrace{\int_L f N^d_{m,p_d}(x)\ dx}_{f^d_m} \\ &= f^s_j f^d_m \qquad \begin{matrix} j = 1,\dots,n_s \\ m = 1,\dots,n_d. \end{matrix}\end{aligned} \tag{52}$$

Due to the boundary conditions of equation (44), the first two coefficients of the vector $u_l(\theta)$, i.e. $u_1(\theta)$ and $u_2(\theta)$, are equal to zero, because $u_1(\theta)$ represents the deflection and $u_2(\theta) - u_1(\theta)$ the slope at the clamped end. Thus, for equation (50) it holds

$$u_{i1} = u_{i2} = 0 \tag{53}$$

for $i = 1,\dots,n_s$,which leads to a reduced system of equation (50) with dimension $n_d(n_s - 2) \times n_d(n_s - 2)$. Solving the reduced system, $n_d(n_s - 2)$ coefficients of $\tilde{u}(x,\theta)$ are determined, where as the control variables u_{in_d} represents the stochastic beam tip deflection

$$\tilde{u}_L(\theta) = \sum_{i=1}^{n_s} u_{in_d} N^s_{i,p_s}(U(\theta)). \tag{54}$$

Further, the relative mean error at the free end can then be computed by

$$\varepsilon_{\text{mean}} = \left|\frac{\mathbf{E}\left[\tilde{u}_L\right] - \mathbf{E}\left[u(L,\theta)\right]}{\mathbf{E}\left[u(L,\theta)\right]}\right| \tag{55}$$

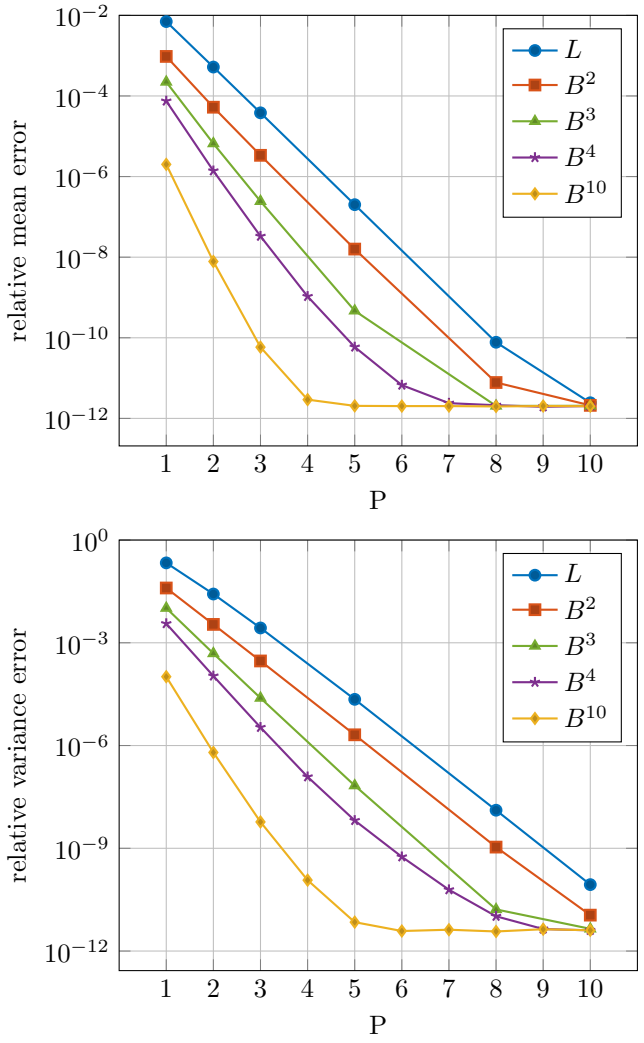

Figure 11: Relative mean and variance error at the beam tip solved by Legendre and B-spline chaos with uniformly distributed beam rigidity.

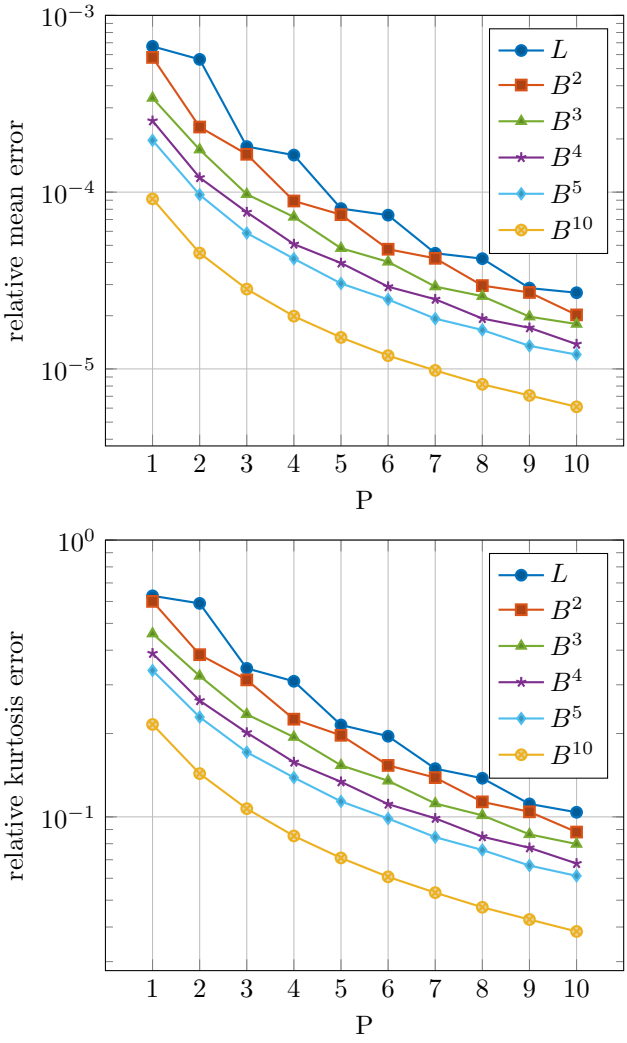

Figure 12: Relative mean and kurtosis error at the beam tip solved by Legendre and B-spline chaos with normally distributed beam rigidity.

with

$$\begin{aligned}\mathbf{E}\left[\tilde{u}_L\right] &= \sum_{i=1}^{n_s} u_{in_d}\,\mathbf{E}\left[N^s_{i,p_s}(U(\theta))\right] \\ &= \sum_{i=1}^{n_s} u_{in_d}\int_{[0,1]} N^s_{i,p_s}(u)\; dF_U(u) \end{aligned} \tag{56}$$

and, considering (45) with $x = L$,

$$\mathbf{E}\left[u(L,\theta)\right] = \mathbf{E}\left[\frac{f\,L^4}{8\,W(\theta)}\right] = \frac{f\,L^4}{8}\int_{S_W}\frac{1}{w}\;dF_W(w). \tag{57}$$

Analogously, the relative variance and kurtosis error are evaluated in common fashion.

For the numerical implementation of the preceding analysis fourth order B-splines with four elements defined by the knot vector $\Xi^d = [\ 0\ 0\ 0\ 0\ 0.25\ 0.5\ 0.75\ 1\ 1\ 1\ 1\ ]$ were used, i.e. $p_d = 4$, $nel_d = 4$ and $k_d = p_d - 1$, resulting in eight ($n_d = m_d - p_d - 1 = 8$) degrees of freedom; m_d denotes the number of knots in Ξ^d - compare Fig. 2.

4.3.1. Uniformly distributed beam rigidity

Let $W \sim \mathcal{U}([0.5, 1.5])$ and $f \equiv 1$. Since the B-spline chaos is optimal for a uniform distribution, the approximation (47) is exact for $n_w > 1$, e.g.

$$W(\theta) \equiv \widetilde{W}(\theta) = \sum_{k=1}^{2} w_k N^w_{k,1}(U(\theta)) \tag{58}$$

with $w_1 = 0.5$, $w_2 = 1.5$ and knot vector $\Xi^w = [\ 0\ 0\ 1\ 1\ ]$. Further, the exact mean solution is given by

$$\begin{aligned}\mathbf{E}\left[u(L,\theta)\right] &= \frac{1}{8}\int_{0.5}^{1} .5\frac{1}{w}\;dw \\ &= \frac{1}{8}\big(\log(1.5) - \log(0.5)\big) \\ &\approx 0.137326536083514. \end{aligned} \tag{59}$$

Exponential h-p convergence for the first two central moments of the beam tip deflection are shown in Fig. 11. The results are found in good agreement with the previous example from section 4.2. The relative mean and variance

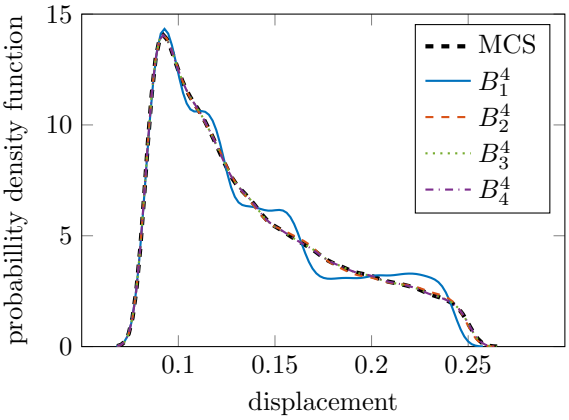

Figure 13: Probability density function approximations of the cantilever beam tip deflection with uniformly distributed beam rigidity.

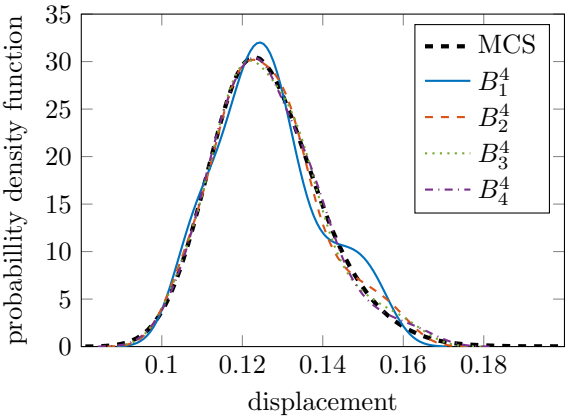

Figure 14: Probability density function approximations of the cantilever beam tip deflection with normally distributed beam rigidity.

error are plotted for a different number of stochastic elements as well as the classical Legendre chaos, which performs the worst. The mean error of the four element B-spline chaos (B^4) reach the deterministic approximation error of about 10^{-13} for $p_s \leq 7$. When ten stochastic elements are considered even only fourth order B-splines are required. In general, the relative mean errors converge faster than the errors of higher moments.

4.3.2. Normal distributed beam rigidity

In this section the distribution of the random input W is assumed to be normal, i.e. $W \sim \mathcal{N}(1, 0.1)$, and $f \equiv 1$. As can be seen in section 4.1.3, the B-spline chaos is not optimal for a normal distribution. Thus, the solution quality of $\tilde{u}(x, \theta)$ also depends on the approximation $\widetilde{W}(\theta)$. Therefore, $p_w = 10$, $nel_w = 10$ and $k_w = 0$ are chosen in order to reach high accuracy. Further, the exact mean solution of (44) is

$$\mathbf{E}\left[u(L,\theta)\right] = \frac{1}{8}\int_{-\infty}^{\infty} \frac{1}{\sqrt{2\pi\ 0.1^2}\ w} \exp(-\tfrac{(w-1)^2}{0.1^2})\ dw \approx 0.126289521160065, \tag{60}$$

which was solved numerically.
Fig. 12 shows the *h-p* convergence in the stochastic space of the first and fourth central moment at the beam tip. The beam rigidity $W(\theta)$ is represented by the non-optimal B-spline chaos which is an indication for the lower convergence rate in comparison with the optimal representation in section 4.3.1. However, the B-spline chaos still dominates the Legendre chaos. Further, it is remarkable that even for higher orders the high moments do not deteriorates which is a general problem for the Hermite chaos [18].

4.3.3. Monte Carlo simulation

In order to assess the significance of the numerical results obtained from the B-spline chaos the beam problem is threated by a Monte Carlo simulation. Realizations of the beam rigidity $W(\theta)$ are computed and for each realization the associated deterministic problem (48) is solved. The resulting density function of the beam tip deflection for $W \sim \mathcal{N}(1, 0.1)$ and $W \sim \mathcal{U}([0.5, 1.5])$ are plotted in Fig. 13 and Fig. 14, respectively. Comparisons with different B-spline types show a satisfactory level of accuracy for $p_s > 1$ in both cases. Nevertheless, for the uniform input better results are achieved which coincides with the error plots from section 4.1 and 4.2. The probability density functions in Fig. 13 and Fig. 14 are estimated by a normal kernel smoothing function with bandwidth 0.005 and 10000 samples.

5. Concluding remarks

In this paper the potential of B-spline chaos has been demonstrated. Weak convergence for arbitrary random variables has been shown and substantiated by several numerical examples. Correspondingly, the B-spline approach has been found optimal for uniform input and generalizes the Legendre multi-element chaos of Wan and Karniadakis [8]. Further, it has been found that the smoothness property of B-spline basis functions improves significantly the efficiency when decomposing the random space, which comes to a greater extent if the dimensionality is increased. As a first example, to show the versatility and flexibility of the B-spline chaos uniform, beta, normal, and exponential distributed random variables have been approximated. Varying the polynomial degree, number of elements and also the continuity over element boundaries are powerful tools to treat arbitrary non-uniform random inputs. Afterwards, a first order stochastic ordinary differential equation has been investigated within a Galerkin framework to address long-time integration problems. Exponential *h-p* convergence has been achieved for uniform input. Note that Wan and Karniadakis [8] have stated that the efficiency of ME-gPC is reduced significantly by the rapidly increasing number of random elements for high-dimensional problems; the results reported herein indicate

that the B-spline chaos can overcome this drawback. Further, a one dimensional static beam problem under uniformly and normal distributed random flexural rigidity has been considered using Galerkin projections. h-p convergence has been demonstrated even for higher moments. The accuracy of the B-spline technique is also established by pertinent Monte Carlo simulations.

References

[1] R. Ghanem, P. Spanos, Stochastic Finite Elements: A Spectral Approach, Dover Publications, INC., Mineola, New York, revised edn., 2003.

[2] M. Grigoriu, Stochastic Calculus: Applications in Science and Engineering, Birkhäuser, ISBN 0-8176-4242-0, 2003.

[3] R. Ghanem, P. Spanos, A stochastic Galerkin expansion for nonlinear random vibration analysis, Probabilistic Engineering Mechanics 8 (3-4) (1993) 255–264, ISSN 0266-8920, doi:10.1016/0266-8920(93)90019-R.

[4] G. Stefanou, The stochastic finite element method: Past, present and future, doi:10.1016/j.cma.2008.11.007, 2009.

[5] N. Wiener, The homogeneous chaos., Amer. J. Math 60897 (4) (1938) 936, ISSN 00029327, doi:10.2307/2371268.

[6] R. H. Cameron, W. T. Martin, The Orthogonal Development of Non-Linear Functionals in Series of Fourier-Hermite Functionals, The Annals of Mathematics 48 (2) (1947) 385, ISSN 0003486X, doi:10.2307/1969178.

[7] D. Xiu, G. E. Karniadakis, The Wiener–Askey Polynomial Chaos for Stochastic Differential Equations, SIAM Journal on Scientific Computing 24 (2) (2002) 619–644, ISSN 1064-8275, doi:10.1137/S1064827501387826.

[8] X. Wan, G. E. Karniadakis, An adaptive multi-element generalized polynomial chaos method for stochastic differential equations, Journal of Computational Physics 209 (2) (2005) 617–642, ISSN 0021-9991, doi:10.1016/J.JCP.2005.03.023.

[9] X. Wan, G. E. Karniadakis, Multi-Element Generalized Polynomial Chaos for Arbitrary Probability Measures, SIAM Journal on Scientific Computing 28 (3) (2006) 901–928, ISSN 1064-8275, doi:10.1137/050627630.

[10] X. Wan, G. E. Karniadakis, Long-term behavior of polynomial chaos in stochastic flow simulations, Computer Methods in Applied Mechanics and Engineering 195 (41-43) (2006) 5582–5596, ISSN 0045-7825, doi:10.1016/J.CMA.2005.10.016.

[11] X. Wan, G. E. Karniadakis, Solving elliptic problems with non-Gaussian spatially-dependent random coefficients, Computer Methods in Applied Mechanics and Engineering 198 (21-26) (2009) 1985–1995, ISSN 00457825, doi:10.1016/j.cma.2008.12.039.

[12] G. Kewlani, J. Crawford, K. Iagnemma, A polynomial chaos approach to the analysis of vehicle dynamics under uncertainty, Vehicle System Dynamics 50 (5) (2012) 749–774, ISSN 0042-3114, doi:10.1080/00423114.2011.639897.

[13] J. Le Meitour, D. Lucor, J. C. Chassaing, Prediction of stochastic limit cycle oscillations using an adaptive polynomial chaos method, J. Aero. Struct. Dyn. 2 (1).

[14] E. Sarrouy, O. Dessombz, J.-J. Sinou, Piecewise polynomial chaos expansion with an application to brake squeal of a linear brake system, Journal of Sound and Vibration 332 (3) (2013) 577–594, ISSN 0022460X, doi:10.1016/j.jsv.2012.09.009.

[15] M. Gerritsma, J. B. van der Steen, P. Vos, G. Karniadakis, Time-dependent generalized polynomial chaos, Journal of Computational Physics 229 (22) (2010) 8333–8363, ISSN 00219991, doi:10.1016/j.jcp.2010.07.020.

[16] B. Chouvion, E. Sarrouy, Development of error criteria for adaptive multi-element polynomial chaos approaches, Mechanical Systems and Signal Processing 66-67 (2016) 201–222, ISSN 10961216, doi:10.1016/j.ymssp.2015.05.007.

[17] R. Ghanem, Stochastic Finite Elements with Multiple Random Non-Gaussian Properties, Journal of Engineering Mechanics 125 (1) (1999) 26–40, ISSN 0733-9399, doi:10.1061/(ASCE)0733-9399(1999)125:1(26).

[18] R. V. Field, M. Grigoriu, On the accuracy of the polynomial chaos approximation, in: Probabilistic Engineering Mechanics, vol. 19, Elsevier, ISBN 0266-8920, ISSN 02668920, 65–80, doi:10.1016/j.probengmech.2003.11.017, 2004.

[19] T. J. Hughes, J. A. Cottrell, Y. Bazilevs, Isogeometric analysis: CAD, finite elements, NURBS, exact geometry and mesh refinement, doi:10.1016/j.cma.2004.10.008, 2005.

[20] G. Sangalli, T. Hughes, L. Beirão da Veiga, F. Auricchio, A. Reali, Isogeometric Collocation Methods, Mathematical Models and Methods in Applied Sciences 20 (11) (2010) 2075–2107, ISSN 0218-2025, doi:10.1142/s0218202510004878.

[21] J. Cottrell, A. Reali, Y. Bazilevs, Isogeometric analysis of structural vibrations, Computer Methods in Applied Mechanics and Engineering 195 (41-43) (2006) 5257–5296, ISSN 0045-7825, doi:10.1016/J.CMA.2005.09.027.

[22] Y. Bazilevs, V. M. Calo, T. J. R. Hughes, Y. Zhang, Isogeometric fluid-structure interaction: Theory, algorithms, and computations, Computational Mechanics 43 (1) (2008) 3–37, ISSN 01787675, doi:10.1007/s00466-008-0315-x.

[23] J. Cottrell, J. Evans, S. Lipton, M. Scott, T. Sederberg, Isogeometric analysis using T-splines, Computer Methods in Applied Mechanics and Engineering 199 (5-8) (2010) 229–263, ISSN 0045-7825, doi:10.1016/J.CMA.2009.02.036.

[24] F. Auricchio, L. Beirão da Veiga, T. Hughes, A. Reali, Isogeometric collocation for elastostatics and explicit dynamics, Computer Methods in Applied Mechanics and Engineering 249-252 (2012) 2–14, ISSN 0045-7825, doi:10.1016/J.CMA.2012.03.026.

[25] G. Bhardwaj, I. Singh, B. Mishra, Stochastic fatigue crack growth simulation of interfacial crack in bi-layered FGMs using XIGA, Computer Methods in Applied Mechanics and Engineering 284 (2015) 186–229.

[26] T. D. Hien, H. C. Noh, Stochastic isogeometric analysis of free vibration of functionally graded plates considering material randomness, Computer Methods in Applied Mechanics and Engineering 318 (2017) 845–863, ISSN 00457825, doi:10.1016/j.cma.2017.02.007.

[27] K. Li, W. Gao, D. Wu, C. Song, T. Chen, Spectral stochastic isogeometric analysis of linear elasticity, Computer Methods in Applied Mechanics and Engineering 332 (2018) 157–190, ISSN 00457825, doi:10.1016/j.cma.2017.12.012.

[28] D. Xiu, Numerical Methods for Stochastic Computations: A Spectral Method Approach, Princeton University Press, ISBN 9780691142128, 2010.

[29] R. Ghanem, P. D. Spanos, Polynomial Chaos in Stochastic Finite Elements, Journal of Applied Mechanics 57 (1) (1990) 197–202, ISSN 0021-8936, doi:10.1115/1.2888303.

[30] R. T. Farouki, LegendreBernstein basis transformations, Journal of Computational and Applied Mathematics 119 (2000) 145–160, ISSN 03770427, doi:10.1016/S0377-0427(00)00376-9.